ELSEVIER

NeuroImage

www.elsevier.com/locate/ynimg
NeuroImage 35 (2007) 1409 – 1423

Three-dimensional cerebral vasculature of the CBA mouse brain: A magnetic resonance imaging and micro computed tomography study

A. Dorr,[a] J.G. Sled,[b] and N. Kabani[a,*]

[a]*Sunnybrook Health Sciences Centre, 3080 Yonge Street, Suite 6020, P.O. Box 89, Toronto, ON, Canada M4N 3N1*
[b]*Hospital for Sick Children, Toronto, ON, Canada*

Received 1 August 2006; revised 7 December 2006; accepted 8 December 2006
Available online 23 January 2007

Studies of mouse cerebral vasculature to date have focused on the circle of Willis without examining the morphological distribution of blood vessels through the rest of the brain. Since mouse models are frequently used in brain-related studies, there is a need for a comprehensive cerebral vasculature atlas for the mouse with an emphasis on the location of vessels with respect to neuroanatomical structures, the watershed regions associated with specific arteries, as well as a consistent nomenclature of the cerebral vessels. This article describes such an atlas, based on a combination of magnetic resonance and computed tomography technology to yield high-resolution volumetric and vasculature data on CBA mouse. This three-dimensional vasculature dataset provides an anatomical resource for future mouse studies.

Introduction

The mouse is widely used in biological research, and as such, much is known about its visceral and cerebral anatomy. However, the cerebro-vasculature system is sparsely described. Most mouse cerebral vascular studies, motivated by a need to control variability in ischemia models, have focused on the circle of Willis (Beckmann, 2000; Beckmann et al., 2003; Kitagawa et al., 1998; Maeda et al., 1998; Okuyama et al., 2004; Ward et al., 1990). The growing use of mouse models for a diverse range of neurological applications has created a need for a comprehensive cerebral vasculature atlas.

In the absence of a mouse cerebral vascular atlas, existing vascular atlases from rats (Scremin, 1995; Greene, 1955) and guinea pigs (Majewska-Michalska, 1994 1995, 1997a,b,c, 1998) have been used as guidelines. Most of the comparisons between mouse and rat have focused on the circle of Willis (Beckmann, 2000; Beckmann et al., 2003; Kitagawa et al., 1998; Okuyama et al., 2004), a structure that is highly conserved between these two members of the subfamily Murinae (Wilson and Reeder, 2006). This paper traces vascular anatomy beyond the circle of Willis and presents the morphology of brain vasculature throughout the cortical and deep structures of the brain.

With the advancement of technology, new ways have developed to observe many aspects of rodent neuroanatomy and cerebral vasculature. It is now possible to visualize brain vasculature in vivo using magnetic resonance angiography (Beckmann et al., 1999, 2003; Beckmann, 2000; Krucker et al., 2004; Lin et al., 1997; Miraux et al., 2004; Reese et al., 1999). Vascular corrosion casting of fixed specimens allows more detailed examination (Krucker et al., 2004) that when combined with electron microscopy allows superficial capillary structure to be visualized (Ohtake et al., 2004). High-resolution X-ray computed tomography (microCT) (Jorgensen et al., 1998) allows three-dimensional (3D) visualization and analysis of intact brain specimens with vessels 20 μm in diameter and larger resolved (Marxen et al., 2004). MicroCT allows visualization of the vasculature without the need for macerating the tissue by perfusing the specimen with an X-ray opaque contrast agent. The 3D images produced by microCT have a distinct advantage over 2D histological slices, as one can unambiguously identify a vessel along its entire length from the vessel's origin to the terminal region. A similar analysis of histological slices requires many sections and may lead to ambiguous situations due to tissue shrinkage or vessel branching. MicroCT scans can be used in conjunction with high-resolution MRI scans of the brain, enabling one to align the CT image with the MRI in order to determine the exact placement of the cerebral vessels in relation to the brain structures around the vessel of interest. Vessel contrast relative to noise determines the smallest vessels that can be

Abbreviations: ACA, anterior cerebral artery; AchA, anterior choroid artery; azACA, azygos of the ACA (fusion of the two ACA); azPA, azygos pericallosal artery; BA, basilar artery; IC, internal carotid; MCA, middle cerebral artery; PCA, posterior cerebral artery; PcomA, posterior communicating artery; SCA, superior cerebellar artery.

* Corresponding author. Fax: +1 416 482 3807.
E-mail address: nkabani@sten.sunnybrook.utoronto.ca (N. Kabani).
Available online on ScienceDirect (www.sciencedirect.com).

1053-8119/$ - see front matter © 2006 Elsevier Inc. All rights reserved.
doi:10.1016/j.neuroimage.2006.12.040

detected in the CT data. As this contrast drops rapidly for vessels smaller in diameter than the point spread function of the imaging system, the image resolution and smallest detectable vessel are similar. In a recent study, Marxen et al. reported that vessels 22 μm in diameter could be resolved on a similar microCT scanner (Marxen et al., 2004).

This study used a combination of microCT and high-resolution MRI to trace three-dimensional cerebral vasculature patterns in CBA mouse and showed the normal placement of the major arteries and their visible branches, along with the brain structures they feed. This is the first 3D atlas of the cerebral vasculature in mice. It can be used as a guide for normal anatomy and for identifying deviation from normal patterns as a result of diseases.

Methods

An average brain volume was created using the magnetic resonance images of the four mice.

Specimen preparation

In this study, four CBA male mice (ages 6 and 16 months), obtained from the National Institute on Aging, Bethesda, MD, USA were used. Mice were anesthetized with an intraperitoneal injection of ketamine (50 mg/kg) and xylazine (10 mg/kg). Heparinized PBS (1 unit heparin/ml) at 37 °C was injected into the left ventricle of the heart and drained from the right atrium. The circulation was then filled with a radio-opaque silicone rubber (Microfil® MV-122, Flow-Tech Inc.) at a constant pressure of 160 mm Hg and left to polymerize for 90 min. Next, the heads were removed along with the skin, lower jaw, ears and the cartilaginous nose tip. The remaining skull structures were allowed to fix in 4% paraformaldehyde at 4 °C for 12 h. Following a further incubation period of 5 days in phosphate-buffered solution (PBS) and 0.01% sodium azide at 15 °C, the skulls were transferred to a PBS and 2 mM Prohance® (Bracco Diagnostics Inc., Princeton, NJ) solution for at least 7 days at 15 °C. MR imaging occurred 12 to 21 days postmortem.

MR imaging

A four-channel 7.0-T MR scanner (Varian Inc., Palo Alto, CA, USA) with a 6-cm inner bore diameter gradient set was used to acquire anatomical images of brains within skulls. Prior to imaging, the skulls were removed from the contrast agent solution and placed into plastic tubes filled with a proton-free susceptibility-matching fluid (Fluorinert FC-77, 3 M Corp., St. Paul, MN). Custom-built, 12-mm over-wound uniform solenoid coils were used to image three brains in parallel. The parameters used in the scans were optimized for grey/white matter contrast: T2-weighted, 3D fast spin-echo sequence, with TR/TE = 325/32 ms, four averages, field-of-view $12 \times 12 \times 25$ mm^3 and matrix size = $780 \times 432 \times 432$ resulting in an image with 32 μm isotropic voxels in a 14-h scan time (Nieman et al., 2005; Henkelman et al., 2006).

MicroCT imaging

In preparation for scanning with microCT, the brains were removed from the skulls and mounted in 1% agar. Each vascular image volume was acquired with 20 μm isotropic resolution using a GE eXplore Locus SP specimen scanner. Images were obtained from 720 views over a 360° rotation in 2 h with an X-ray tube current of 80 μA and voltage of 80 kV p.

Image processing

A representative image of the CBA mouse neuroanatomy with improved soft tissue contrast was obtained by averaging together the MRI scans of the four individual mice using a technique that removes smooth inter-specimen anatomical variation (Kovacevic et al., 2005). This technique, which employs automated non-linear co-registration of the 3D images, centers the resulting average in the sense that the degree of spatial transformation between the individual images and their average is minimized. The average image was rotated into a standard orientation for ease of segmentation and visualization.

As variation among fine vessels of the neurovasculature prevents meaningful averaging of the CT images, a single 6-month-old specimen was selected for mapping of the vessel network. The selected microCT image was aligned with the corresponding MRI using 33 manually identified landmarks located at the branch points of major vessels. The silicone rubber contrast agent causes vessels to appear dark on MRI and bright on CT. Tensor cubic B-spline approximation was used to compute a non-linear transformation based on the landmarks so as to bring the MRI and CT images into alignment and remove any distortion to the specimen that may have been introduced by removing the skull. The CT image was then aligned with the average MRI using the previously computed transformation.

Segmentation process

The boundaries of major anatomical regions described previously for the mouse (Franklin and Paxinos, 2001; Ma et al., 2005) were outlined in three dimensions on a slice by slice basis using Display, an image analysis software developed at the McConnell Brain Imaging Centre of the Montreal Neurological Institute.

The selected CT image was used in combination with the average MRI to identify each voxel corresponding to a given artery or vein along with the attached network of minor vessel. All the named vessels described in our atlas were verified to be present in the same configuration in all four specimens. The illustrations presented in the atlas were created by volume rendering the CT image data from those voxels identified as a given vessel using the Amira package (Mercury Computing Systems, San Diego, CA). This approach gives the vascular networks a semi-transparent appearance and provides a more accurate presentation of the vessel dimensions for small vessels. Soft tissue anatomy is presented either as a 2D slice or as a 3D volume rendering of the average MRI.

The vessels of interest are superimposed on slice planes at or near the anatomical location of the artery of interest, where slices were chosen to best show the majority of the artery. In this presentation, portions of the artery located behind the slice plane will not be visible; however, slices were chosen to minimize this effect.

Surface vessels are presented in combination with volume renderings of the MRI data excluding the skull so that these vessels can be located with respect to the brain surface. Some residual discrepancy in the alignment of the CT and MRI data was noted in the area of the brainstem.

Results

The results comprise of the manual segmentation the brain structures followed by a detailed analysis of the cerebral arteries and their innervations.

Manual segmentation of brain structures

Volume renderings of the CBA average mouse brain are shown in Figs. 1A to D. The coronal, sagittal, and horizontal slices of the CBA average mouse brain MRI were used to segment a total of 24 regions bilaterally. Each structure was painted on each slice as presented in Figs. 2A to C.

A. The cortical regions included the (1) olfactory bulb, (2) frontal cortex, (3) parietal–temporal cortex, and (4) occipital cortex.
B. The white matter segmentation consisted of (1) anterior commissure, (2) corpus callosum, (3) optic bundle (including the optic nerve, chiasm and tract), (4) fornix, (5) internal capsule, (6) stria terminalis, (7) stria medularis thalami, and (8) mamillothalamic tract.
C. The deep grey structures included (1) striatum (caudate and putamen), (2) globus pallidus, (3) hippocampus (including the fimbria), (4) amygdala, (5) hypothalamus, (6) thalamus, and the (7) subcortical region for frontal and for parietal regions (including lateral septum, nucleus accumbens, basal forebrain structures such as the nucleus basalis, diagonal band nucleus, substantia innominata, magnocellular nucleus, and medial septal nucleus).
D. The brain stem included the (1) medulla, (2) pons, (3) midbrain, and the (4) cerebellum.
E. The ventricular space was subdivided into lateral and third ventricles.

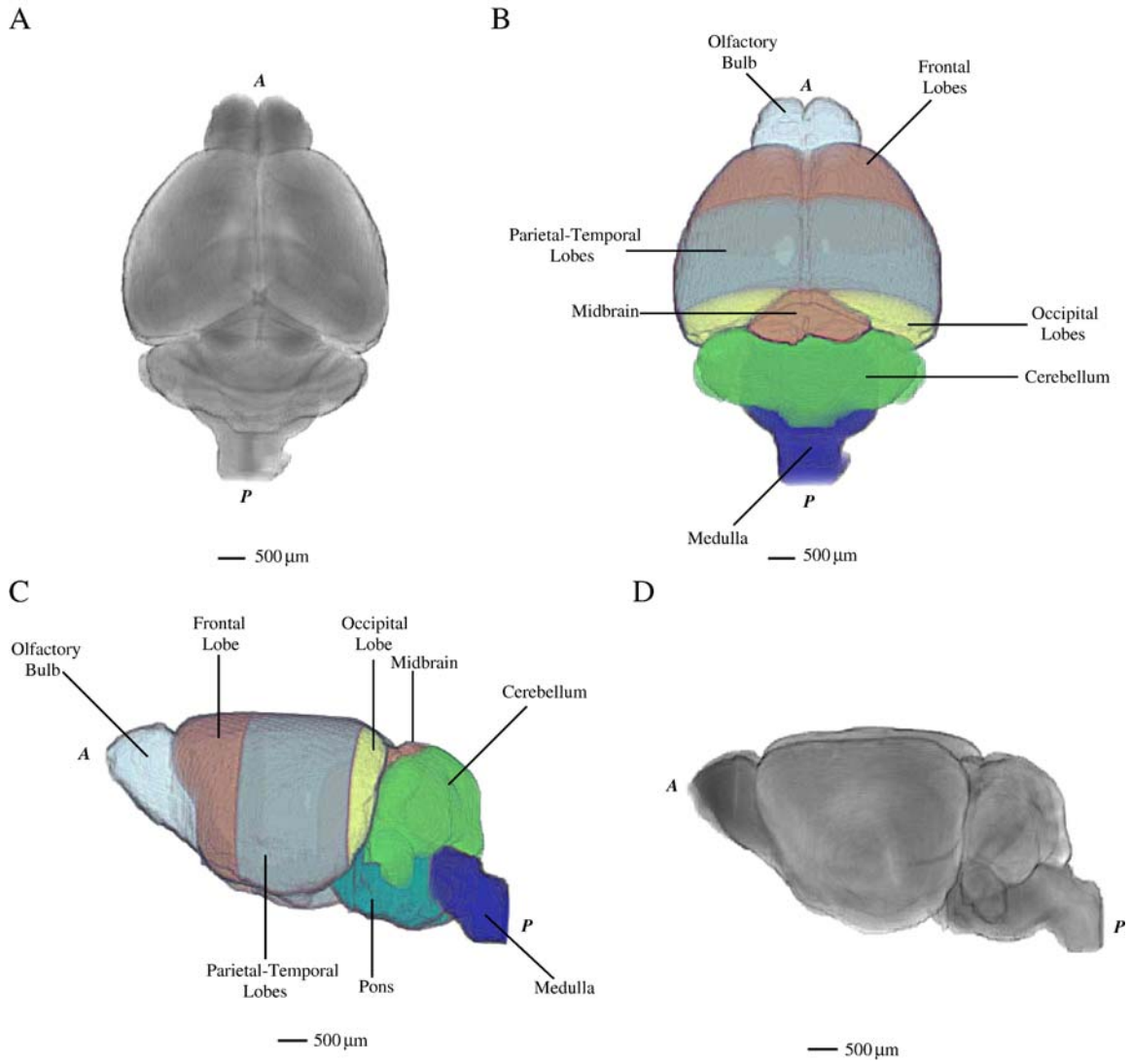

Fig. 1. CBA average mouse brain surfaces: (A) superior view; (B) superior view, with major lobar regions depicted; (C) left view, with major lobar regions depicted; (D) left view. For all panels, A = anterior, P = posterior, scale bar represents 500 µm.

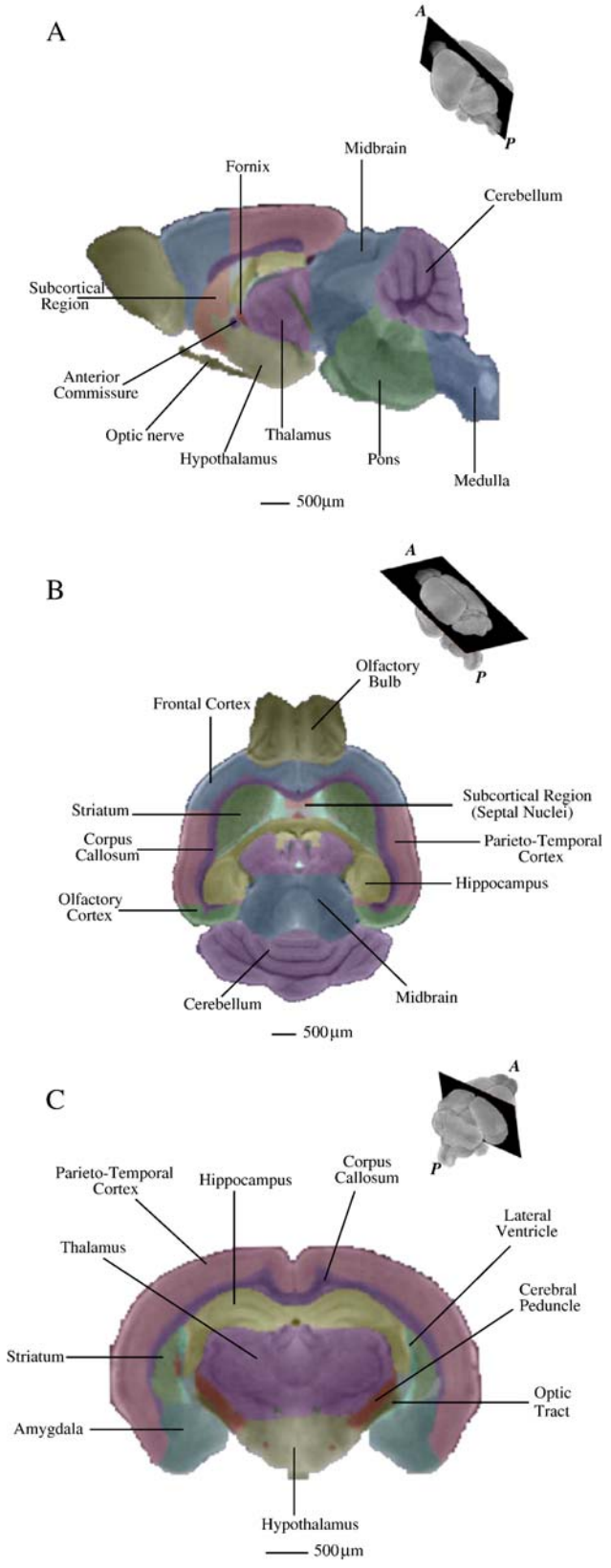

Fig. 2. Manually segmented brain regions on MR brain slices. Inserts represent the level at which the slice of interest was taken: (A) sagittal slice plane, midline; (B) horizontal slice plane; (C) coronal slice plane.

General description of the segmented brain regions

Since the purpose of this article is to discuss vasculature, the description of the segmentation of the brain structures is brief. Figs. 2A to C display the structures in various planes and Figs. 1B and C show the main lobar and brain stem regions on the three-dimensional brain.

The boundaries of the cortical regions were delineated based on the internal structures since there are no major sulcal landmarks in mice to help differentiate the various lobar regions. The most anterior region, the olfactory bulb, a well developed region in mouse brain, ended at the appearance of the corpus callosum in both hemispheres and corresponded with the disappearance of the olfactory bulb nuclei. The olfactory bulb contained the anterior extension of the anterior commissure.

In the coronal view, the anterior portion of the frontal lobe emerged dorsally, surrounding the posterior one-third of the olfactory bulb. Moving posteriorly, the olfactory bulb shrank in size as the frontal lobe expanded to occupy the space.

The frontal lobe region terminated when the anterior commissure was seen to connect the two hemispheres in the coronal section. Structures found in the frontal lobe included the corpus callosum, anterior portion of the anterior commissure, optic nerves, striatum (caudate nucleus and putamen), medial and lateral septal nuclei, the lateral ventricles, and the anterior edge of the optic chiasm. The hypothalamus started in the posterior one-third of the frontal lobe, seen ventral to the anterior commissure and continues into the parietal–temporal region.

The frontal region ended to give way to the parietal–temporal region posteriorly. The parietal and temporal lobes were combined because of lack of any sulcal boundary between the two and also because many internal structures normally present in these lobes in humans were found in the same MRI slices in the mouse brain. The striatum, corpus callosum, lateral ventricle, and optic chiasm continued from the frontal lobe into the parietal–temporal lobe. The hypothalamus, which started in the frontal lobe, continues almost the entire extent of the parieto-temporal region and is located ventral to the thalamus. New structures included the stria terminalis, hippocampus, amygdala, globus pallidus, internal capsule, optic tract, fornix, stria thalamo-medullaris, mamillothalamic tract, thalamus, and the midbrain. The parietal–temporal lobe ended with the termination of the hippocampus.

The occipital lobe, the most posterior lobe of the cerebrum, was the smallest. It contained the posterior extreme of the corpus callosum. This region surrounded the midbrain anterior to the colliculi, as well as a small portion of the anterior pons.

The brain stem was divided into midbrain, pons, and medulla. The pons is easy to identify, as it includes the bulbous pontine nucleus ventrally. The midbrain was located posterior to the thalamus, anterior to the cerebellum, and anterior–dorsal to the pons. The pons continued in the brainstem, ventral to the cerebellum, until the disappearance of the pontine nucleus. The medulla was the most posterior portion of the brain stem.

Manual segmentation of cerebral arteries

Arteries were identified based on their location on the MR images in relation to surrounding brain structures, their branching patterns, and their region of origination and of termination. The rat cerebral vasculature anatomy was mainly used to identify major arteries, as the rat cerebral vasculature is well documented (Greene,

1955; Scremin, 1995) and rats are similar phylogenetically to the mouse, both belonging to the subfamily Murinea of the suprafamily Muroidea (Wilson and Reeder, 2006).

The major blood supply

The major blood supply of the mouse brain comes from two sources. (1) The internal carotid arteries (Table 1) which supply blood to cortical and subcortical regions directly and also through its major branches, including the anterior and middle cerebral arteries as well as parts of the posterior cerebral arteries and (2) the vertebral arteries (Table 2) which supply the arteries of the brainstem and cerebellum and the posterior cerebral artery. The vertebral arteries arise from the subclavian arteries, while the internal carotids arise from the common carotid arteries (Cook, 1965).

Table 1
Nomenclature of the anterior circulation via internal carotid artery

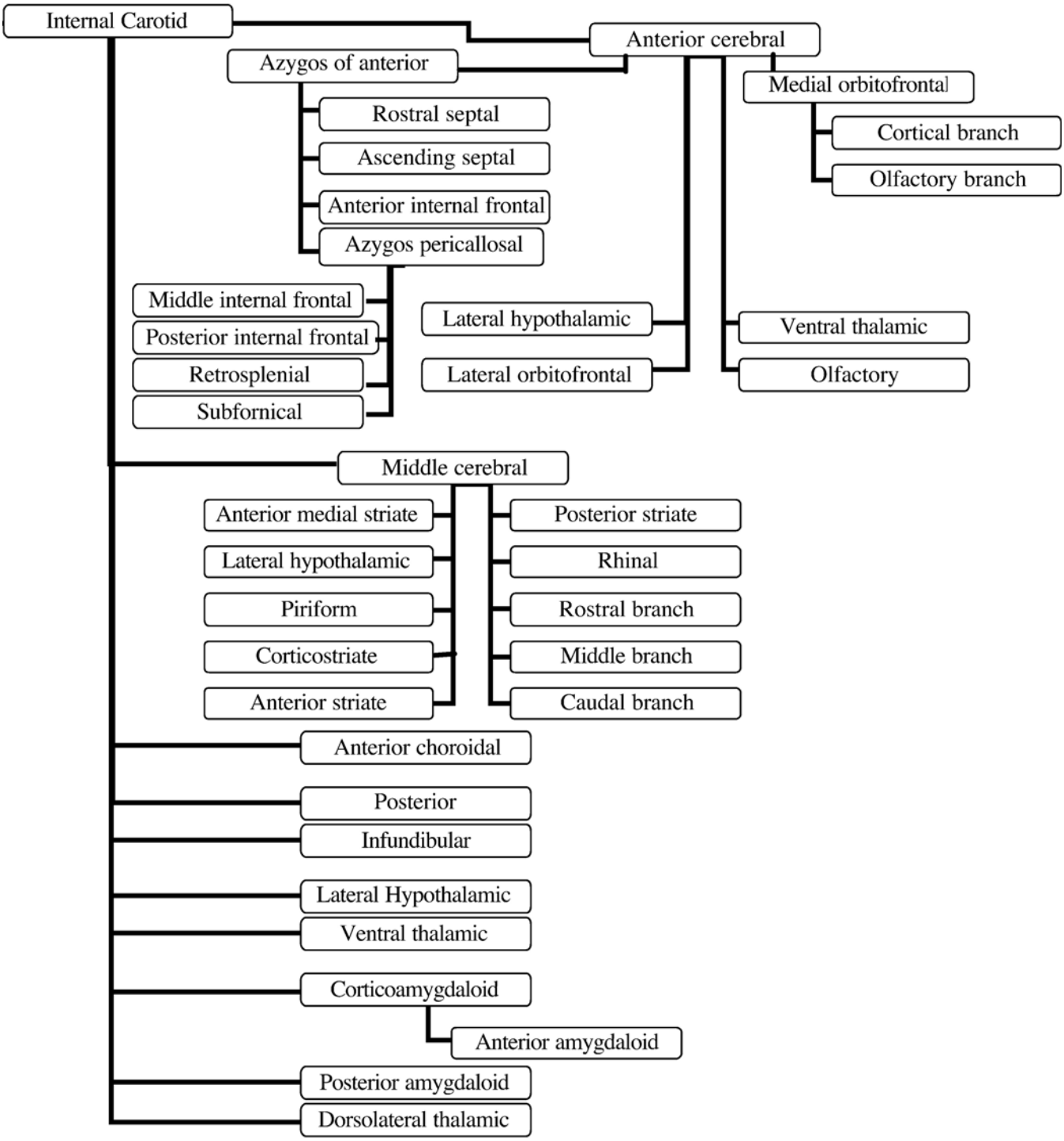

Table 2
Nomenclature of the posterior circulation via the vertebral artery

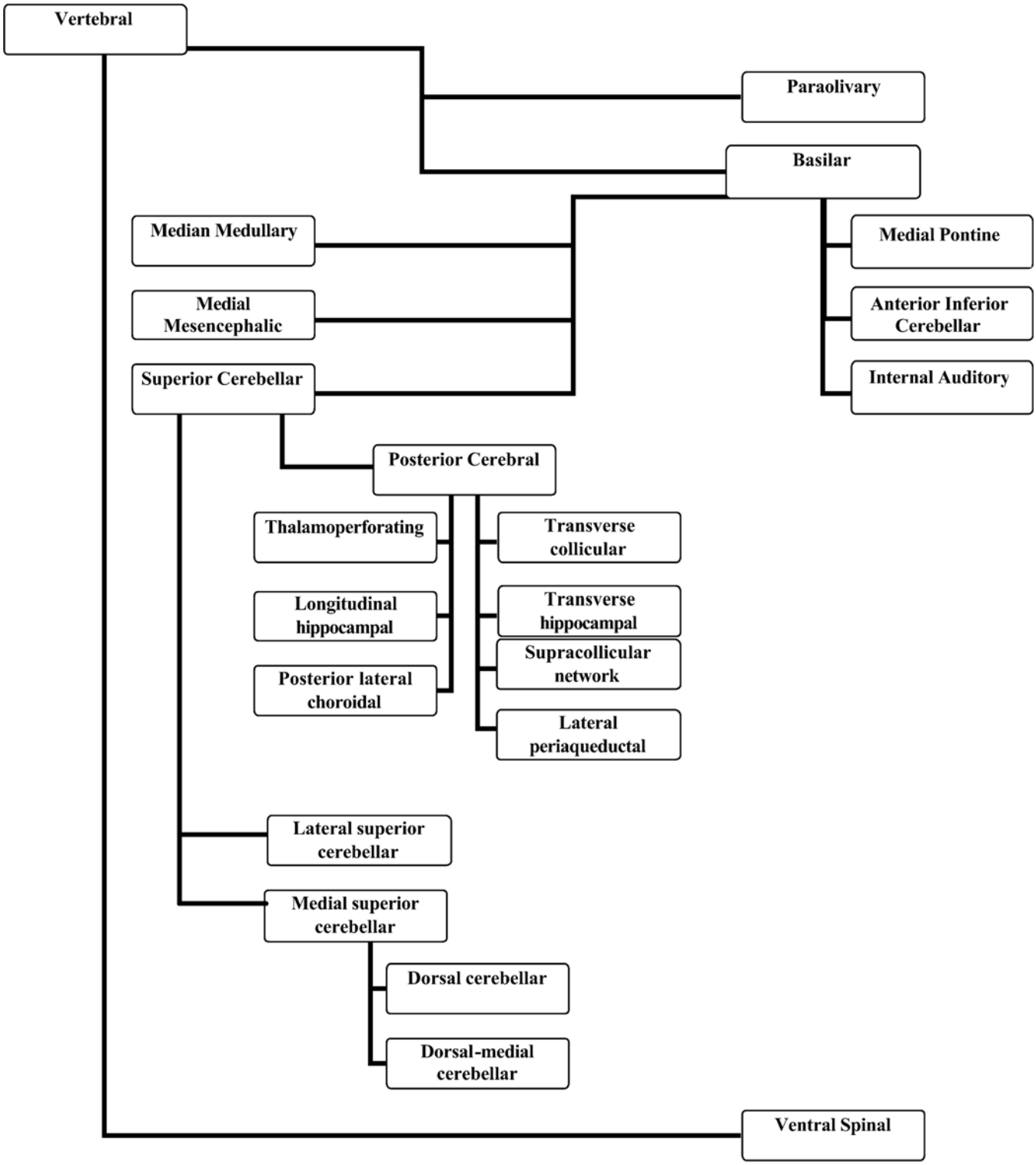

Internal carotid artery

The internal carotid (IC) artery (Figs. 3A and B) is located on the ventral aspect of the brain at the midpoint of the parieto-temporal region, near the hypothalamus. It gave rise to four major arteries including the **posterior communicating artery** (PcomA) posteriorly (Figs. 6A to D), the **middle cerebral artery** (MCA) (Figs. 5A to D), the **anterior cerebral artery** (ACA) anteriorly (Figs. 4A and B), and the **anterior choroidal artery** (AchA) dorsally (Fig. 3B). These arteries are discussed in detail in the following sections.

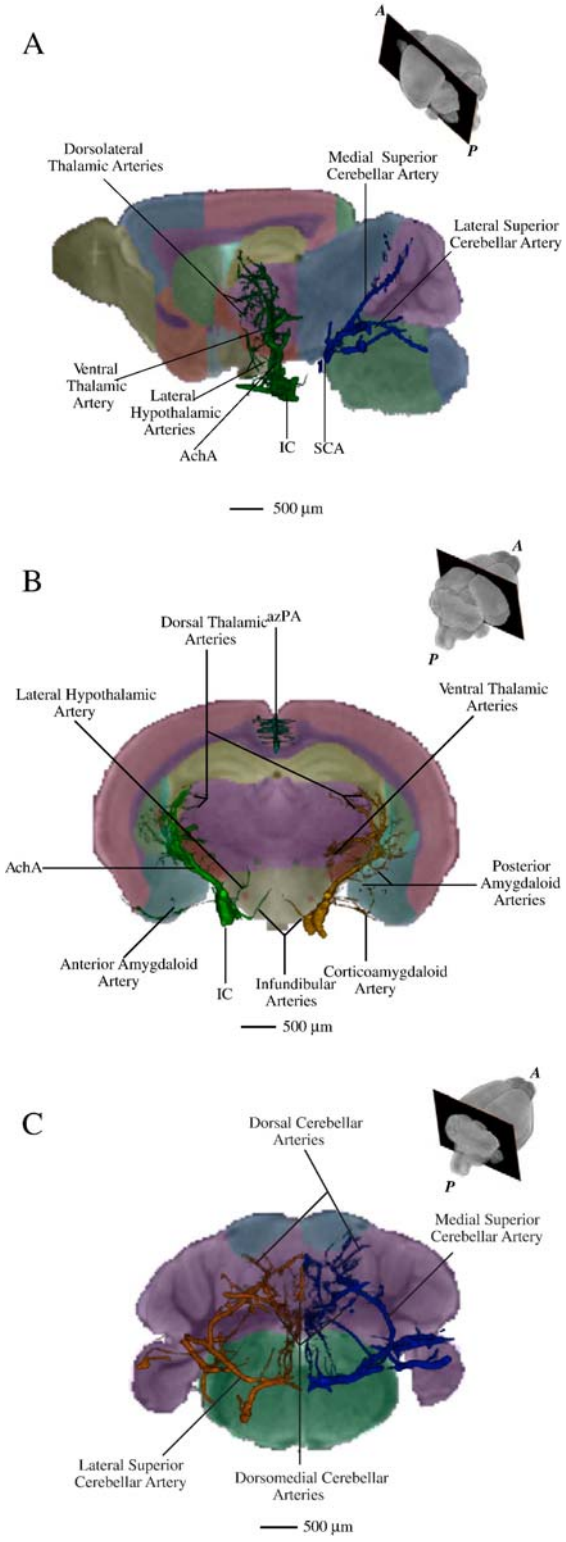

Fig. 3. IC, SCA, and their branches superimposed on slice planes at or near the anatomical location of the artery of interest, where slices were chosen to best show the majority of the artery. Inserts represent the level at which the slice of interest was taken: (A) Sagittal slice plane, left hemisphere view. (B) Coronal slice plane, posterior view. The azPA of the ACA is also visible. (C) Coronal slice plane with the SCA, front view.

In addition the four major arteries described above, the IC also gave off several branches to smaller arteries.

a) The first branches, in the medial direction along the ventral surface of the hypothalamus and then veering dorsally, were identified as the **infundibular arteries** (Fig. 3B).
b) **Lateral hypothalamic arteries** (Fig. 3A) were the next branches, also emerging from the medial edge of the IC, penetrating the lateral edge of the hypothalamus lying dorsal to the artery.
c) **Ventral thalamic arteries** (Fig. 3B) branched off close to the lateral hypothalamic arteries, traveling along the lateral edge of the hypothalamus toward the base of the thalamus.
d) Laterally, the IC gave off the **corticoamygdaloid artery** (Fig. 3B), which heads laterally along the ventral aspect of the brain. This artery gives off small **anterior amygdaloid arteries** (Fig. 3B), which penetrate the overlying cortex to reach the amygdala.
e) Soon after the AchA, a dorsal continuation of the IC, formed, the **posterior amygdaloid arteries** (Fig. 3B) were given off the lateral extent of the AchA. These arteries head laterally and a bit ventrally to penetrate the posterior portion of the amygdala from its dorsal–medial edge.
f) As the AchA continues, it splits into arteries directed more medially and arteries that continue further dorsally. The medially directed arteries are the **dorsolateral thalamic arteries** (Fig. 3A). They supply the thalamus by heading up the lateral edge near the optic tract, penetrating the thalamus from the dorsolateral aspect. The remaining dorsally directed arteries are the continuation of the AchA. These arteries branch toward the lateral ventricle, which lies lateral to the thalamus and optic tract as well as more medial toward the third ventricle and anterior portion of the hippocampus.

The rest of the IC travels ventral and anterior, surrounding most of the hypothalamus, toward its two terminal branches, the middle cerebral artery and the anterior cerebral artery.

Vertebral arteries

The vertebral arteries (VA), as seen in Fig. 6A were located at the level of the medulla, ending at the ponto-medullary junction. The VA gives off several branches, some of which could be distinguished by the microCT scan and are described below.

a) Two large **paraolivary arteries** (Fig. 6A) were found branching from the anterior portion of the vertebral arteries, heading an anterior–lateral direction to supply the inferior olives.
b) The two vertebral arteries fused at the ventral–posterior end of the brainstem, at the level of the medulla, to create one large, midline **basilar artery** (BA) (Fig. 5C) around the ventral midline of the anterior medulla.
c) Just prior to the fusion forming the basilar artery, each VA gives off a short branch medially which join together in the midline to form a single large vessel, called the **ventral spinal artery** (Fig. 5C). This artery supplies the anterior portion of the spinal cord.

The inferior arteries

These include the basilar and the superior cerebellar arteries.

Basilar artery

The basilar artery (BA) is created by the fusion of the two vertebral arteries at the level of the anterior medulla. This artery was found to run on the ventral surface of the brainstem along the midline extending from the anterior medulla to the ponto-medullary junction. Along its path, it gives off small dorsally directed arteries to the overlying brainstem which includes the **median medullary**, the **medial pontine** (Fig. 4A) and the **medial mesencephalic arteries**. Only the medial pontine arteries could be seen clearly in our study, though tiny short branches could be seen from the BA heading in a direction that appears to be toward the midbrain and medulla. **Anterior inferior cerebellar artery (AICA)** (Fig. 6A) branched off laterally from the BA

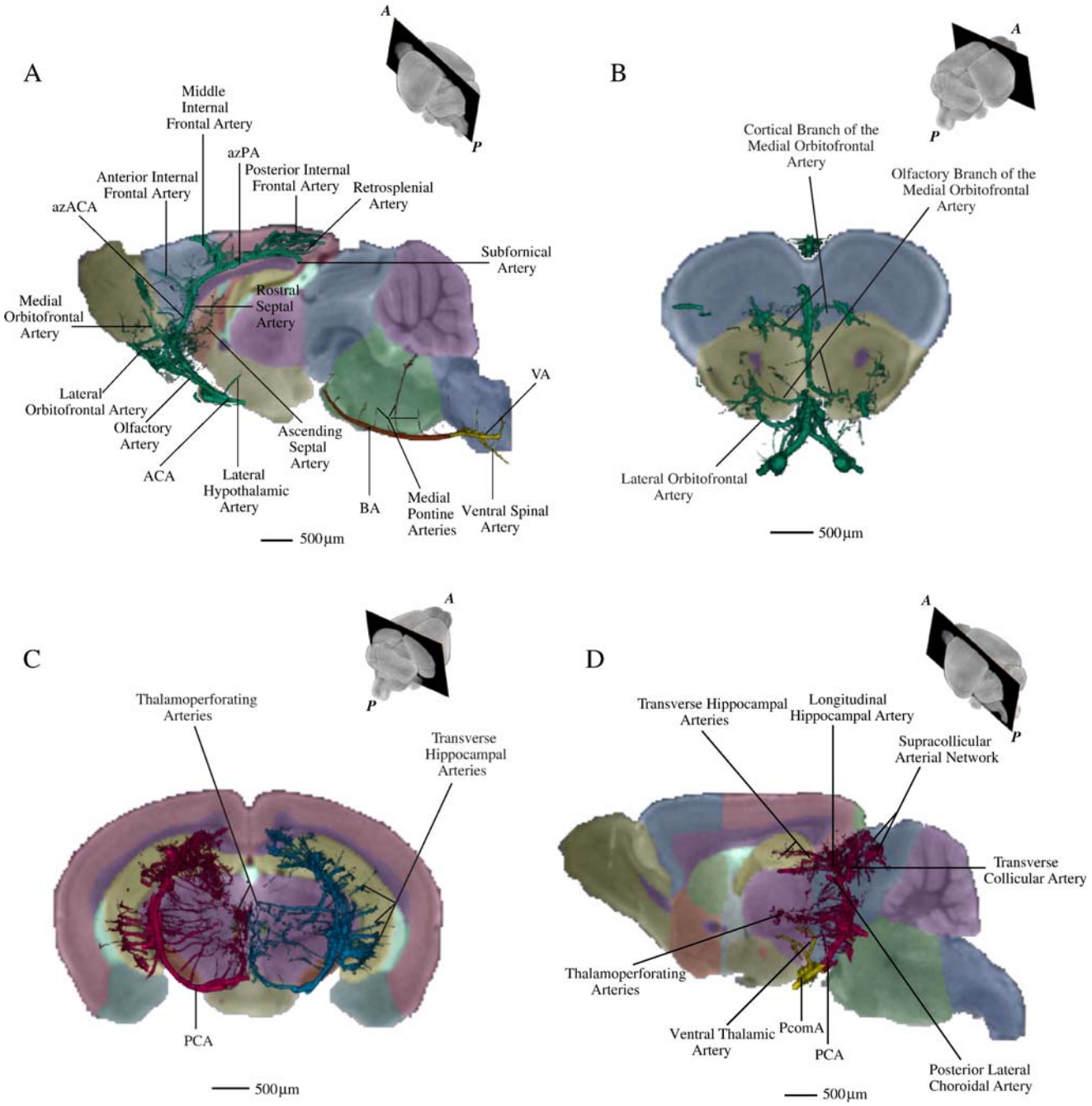

Fig. 4. Slice planes showing the ACA, BA, VA, PCA, PcomA, and their branches, at or near the anatomical location of the artery of interest, where slices were chosen to best show the majority of the artery. Inserts represent the level at which the slice of interest was taken. (A) Saggital slice plane, midline, showing the ACA, BA and VA, as viewed from the left. (B) Coronal slice plane showing the ACA, front view. (C) Coronal slice plane showing the PCA, posterior view. (D) Saggital slice plane showing the PCA and PcomA, left hemisphere view.

around the midpoint of the pons. This artery traveled laterally and dorsally over the lateral edge of the pons, then turned medially to eventually reach the inferior aspect of the cerebellum, thereby supplying the anterior inferior aspect of the cerebellum. Traveling anteriorly along the BA toward the anterior aspect of the pons, two small vessels that may be **internal auditory arteries** (Fig. 6A) branch laterally from the BA. Soon after the appearance of the two internal auditory arteries, around the level of the pons/midbrain junction, the BA was split into two branches, each known as the **superior cerebellar artery** (**SCA**) (Fig. 6A).

Superior cerebellar artery

At its most anterior end, the basilar artery splits into two laterally directed branches thereby forming the two superior cerebellar arteries (SCA). Soon after its creation, the SCA gives off the **posterior cerebral artery** (PCA) (discussed in a later section) anteriorly, as seen in Fig. 6A, and then continues to run laterally, dorsally, and posteriorly to the dorsal–lateral aspect of the pons. Just before reaching the cerebellum, the SCA divided into two major branches, the **lateral SCA** and **medial SCA**, as seen in Fig. 3A. The lateral SCA traveled along the lateral aspect of the cerebellum, through the parafloccular fissure. The medial SCA traveled dorsal–medially up to the top of the cerebellum, where it then gave off a number of **dorsal cerebellar arteries** and **dorsal–medial cerebellar arteries**, visible in Fig. 3C.

The major cerebral arteries

Anterior cerebral artery

The internal carotid bifurcates at the level of the frontal and parieto-temporal junction, to give rise to the anterior cerebral artery (ACA) and the middle cerebral artery (MCA). The ACA (Figs. 4A and B), which supplies the most of the medial aspect of the cerebral cortex (the PCA supplies the posterior medial surface), ran along the ventral aspect of the brain in the trajectory similar to its parent internal carotid artery. The two ACAs, initially continued anteriorly but rapidly veer medially eventually fusing together on the ventral aspect of the frontal lobe (Fig. 6A) to form the **azygos of the anterior cerebral artery** (azACA) (Fig. 4A), just anterior to the optic chiasm. The branches coming off the azACA are discussed later in this section.

As the ACAs veered medially, a pair of arteries branched off the lateral aspect of the ACAs and continued in the same path as the IC. These arteries are called the **olfactory arteries** (Fig. 4A), first appearing just lateral to the optic chiasm, and heading anteriorly to eventually hit the ventral aspect of the olfactory bulb. Just posterior to the emergence of the olfactory arteries, short dorsally directed **lateral hypothalamic arteries** (Fig. 4A) branch from the dorsal aspect of the ACAs, heading toward the overlying hypothalamus.

The **lateral orbitofrontal artery** (Fig. 4B) branched off of the lateral edge of the ACAs, just posterior to the ACA fusion. This artery was best seen on only one hemisphere in Fig. 4B. It ran laterally and anterior to reach the ventral olfactory bulb sending off a branch a bit posterior to reach the anterior nucleus accumbens. The two **medial orbitofrontal arteries**, one for each hemisphere branch off of the anterior side of the dorsally directed azACA. They run anteriorly on the dorsal surface and eventually split into a *cortical branch* and an *olfactory branch*, visible in Fig. 4B. The **cortical branch of the medial orbitofrontal artery** traveled dorsally and a bit posteriorly to the frontal cortex, the anterior cingulate, and the posterior–dorsal part of the olfactory bulb. The **olfactory branch of the medial orbitofrontal artery** was located ventral and anterior to the cortical branch, heading toward the olfactory bulb.

Branches of the azygos of the anterior cerebral artery

In addition to the branches of the medial orbitofrontal arteries from the anterior aspect, many small penetrating arteries also branch off of the posterior aspect of the azACA as it heads towards the dorsal anterior aspect of the corpus callosum. These arteries, as seen in Fig. 4A, head toward the medial and lateral septal nuclei, and are called the **rostral septal artery** and the **ascending septal artery**. The ascending septal artery heads in a characteristic dorsal direction, along the anterior aspect of the septal nuclei. Dorsal to the emergence of the ascending septal artery, the rostral septal arteries emerge from the azACA, heading almost directly posterior, toward the septal nuclei. As the azACA approaches the anterior border of the corpus callosum, a cluster of vessels belonging to the **anterior internal frontal artery** (Fig. 4A) emerge from the anterior side of the azACA, feeding the anterior–medial aspect of the frontal lobe.

The azACA eventually curves over the anterior–dorsal aspect of the corpus callosum and takes a sharp turn posteriorly to form the **azygos pericallosal artery** (**azPA**) for the rest of the artery's extent over the dorsal aspect of the corpus callosum. The azPA and its branches can be seen in Fig. 4A. Shortly after the azACA transitions into the azPA, the azPA gave rise to the network of branches of the **middle internal frontal artery** which primarily supply the posterior–medial aspect of the frontal lobe, with a few branches also extending into the very anterior–medial aspect of the parieto-temporal lobe. Near the end of the azPA, the cluster of vessels belonging to the **posterior internal frontal artery** branches off the azPA to supply a large portion of the medial aspect of the parietal–temporal lobe. At the termination point of the azPA, the **retrosplenial artery** was seen curving dorsal and posteriorly. A **subfornical artery** is expected to curve under the posterior border of the corpus callosum. In our study, a short artery was identified at this location; however, it did not curve completely under the corpus callosum. This may mean that the subfornical artery may exist but perhaps was too small to be seen at the given resolution of the images.

Posterior cerebral artery

The posterior cerebral artery (PCA), visible in Fig. 6C, originated from the anterior portion of the superior cerebellar artery very close to the midline, just anterior to the origin of the SCA from the BA. The PCA initially followed a path similar to the SCA running dorsally but eventually veered anterior to reach the posterior aspect of the cerebrum. **Thalamoperforating artery** originated off the PCA near the midline and a bit lateral and proceeded medially and dorsally to penetrate the ventro-lateral aspect of the thalamus. Anastamoses between thalamoperforating arteries from the two PCAs are visible in Fig. 4C. Bilateral short **posterior communicating artery** (**PcomA**) (Fig. 6C) connected the PCA with the internal carotid. After the junction with the PcomA, the PCA gave off a **transverse collicular artery** (Fig.

4D), directed dorsal–posteriorly toward the inferior colliculus. The PCA also gave off the **longitudinal hippocampal artery** (Fig. 4D) near the origin of, and closely associated to, the transverse collicular artery. The longitudinal hippocampal artery headed dorsally, continuing in the original direction of the PCA, eventually turning anterior to follow the length of the hippocampus. The longitudinal hippocampal artery gave off a number of small **transverse hippocampal arteries** (Fig. 4C), which stem from the parent hippocampal artery in a perpendicular manner. These infiltrate the hippocampus via the hippocampal fissure.

The **posterior lateral choroidal artery** (Fig. 4D) originated from the anterior edge of the longitudinal hippocampal artery and takes a sharp turn anteriorly to follow the hippocampus. Continuing dorsally, the PCA gives off cortical penetrating arteries that supply the cortex of the occipital lobe. In addition, a large **supracollicular arterial network** (Fig. 4D) is formed to supply both the inferior and superior colliculi. Dorsally, **lateral periaqueductal arteries** (not shown) were given off, directed inferior–medially toward the cerebral aqueduct of the midbrain, supplying the periaqueductal region.

Posterior communicating artery

The posterior communicating artery (PcomA) (Fig. 6C) is a very short artery, connecting the internal carotid, located anterior to the PcomA, to the posterior cerebral artery. The PcomAs lie on the ventral–posterior aspect of the cerebrum surrounding the posterior end of the hypothalamus. Along its course, the PcomA gives off a few dorsally and anteriorly directed arteries, the lateral hypothalamic artery and what appear to be ventral thalamic arteries, seen in Fig. 4D. The IC joins the PCA lateral to the PCA origin.

Middle cerebral artery

The MCA branched laterally off of the IC on the ventral–lateral convexity of the cerebrum, just behind the formation of the ACA around the transitional zone from the frontal region to the parieto-temporal region, as shown in Figs. 6A and B. It curved around the ventral portion of the brain in an anterior–lateral direction and traveled dorsally up the side of the brain over the lateral surface of the frontal lobe to reach the top of the brain. In this manner, the MCA supplies much of the lateral surface of the cerebral cortex.

The first set of branches of MCA is the **anterior medial striate artery** (Fig. 5D). These arteries head dorsally to supply the medial edge of the anterior striatum. The striatum includes the putamen and caudate nucleus. Close to the origin of the medial striate arteries, **lateral hypothalamic arteries** (Fig. 5D) are visible, and are similar to those previously described as the branches of the ACA. The **piriform artery** (Fig. 5A) was found to branch off of the MCA, heading in an anterior direction along the ventral aspect of the piriform cortex which constitutes part of the frontal lobe just anterior to the striatum. The **corticostriate artery** (Fig. 5C) was given off close to the origin of MCA, also heading in an anterior direction along the ventral aspect of the piriform cortex and the posterior portion of the olfactory bulb. **Anterior striate and posterior striate arteries** (Fig. 5D) originate from the MCA around the area of the corticostriate artery. However the anterior striate arteries may also originate from the corticostriate arteries. The anterior and posterior striate arteries travel up the lateral edge of the caudate nucleus and putamen, traveling dorsally along the medial aspect of the external capsule. The **rhinal artery** (Fig. 5C) was given off just as the MCA curves around the ventral aspect of the brain. The rhinal artery heads posteriorly and a bit dorsally, near the mid-lateral edge of the cerebrum.

As the MCA travels dorsally toward the top of the brain, it splits into three branches as shown in Fig. 5B: the *rostral* (*or anterior*) *branch*, the *middle branch*, and the *caudal* (*or posterior*) *branch*. The **rostral branch of MCA** heads anterior and dorsal to supply the frontal cortex not supplied by the ACA. The **middle branch of MCA**, traveling dorsally and posteriorly, supplied some of the frontal cortex near its posterior border as well as some of the parietal–temporal cortex. The **caudal branch of MCA** supplies the more dorso-lateral aspect of the parietal–temporal lobe. Short and long cortical branches of the MCA penetrate the cortex underneath its territory, seen in Fig. 5D. Short branches supply the cortical layers, while long branches supply the white matter just beneath the cortex. Many of the side branches from the three main cortical branches of the MCA were hard to decipher, as this area of the brain is also covered extensively by overlapping branches from the superior sagittal sinus and the caudal rhinal vein, draining much of the cortical region supplied by the MCA. In microCT, the contrast is the same for veins and arteries, so only those vessels that could be directly traced back to the main MCA or venous related vessels were labeled as MCA or veins, respectively, while those areas that may have been branches of either the veins or the arteries were left unlabeled.

Circle of Willis

The circle of Willis, an enclosed arterial circle, was located along the ventral aspect of the brain extending from the pons–midbrain junction to the anterior cerebrum and can be seen in Figs. 6A and B. Two major blood sources supply the circle; the vertebral arteries and the internal carotid arteries. The circle itself includes the anterior, middle and posterior cerebral artery, part of the superior cerebellar artery, the internal carotid artery and the posterior communicating artery.

Veins and sinuses

A number of large veins and sinuses were visible on scans. The most anterior vein visible was the **rostral rhinal vein** (Fig. 7A). This vein originates at the dorsal midline of the olfactory bulb–frontal lobe border. As it extends forward, it turns ventral and runs posteriorly following the border between the olfactory bulb and the frontal lobe laterally. The rostral rhinal vein extends to the mid-lateral aspect of the frontal lobe, at the point where the MCA travels dorsal–laterally around the cerebrum. The **caudal rhinal vein** (Fig. 7A) lies in the lateral–medial section of the temporal–parietal lobe and occipital lobe, draining the lateral aspect of these cortices. It also extends to a similar location as the rostral rhinal vein, but appearing posterior to the MCA. Posteriorly, the caudal rhinal vein joins the large **transverse sinus** (Fig. 7B), at the point where the occipital lobe meets the cerebellum. This vessel traveled dorsally from the lateral inferior aspect of the cerebrum to the superior midline, joining the superior sagittal sinus between the two occipital lobes.

Posteriorly, the **sigmoid sinus** (Fig. 7B) emerged from the transverse sinus, traveling over the dorsal cerebellum, lateral to the colliculi. The **medial** and **lateral collicular veins** (Fig. 7D) joined the transverse sinus inferiorly, both laterally surrounding the

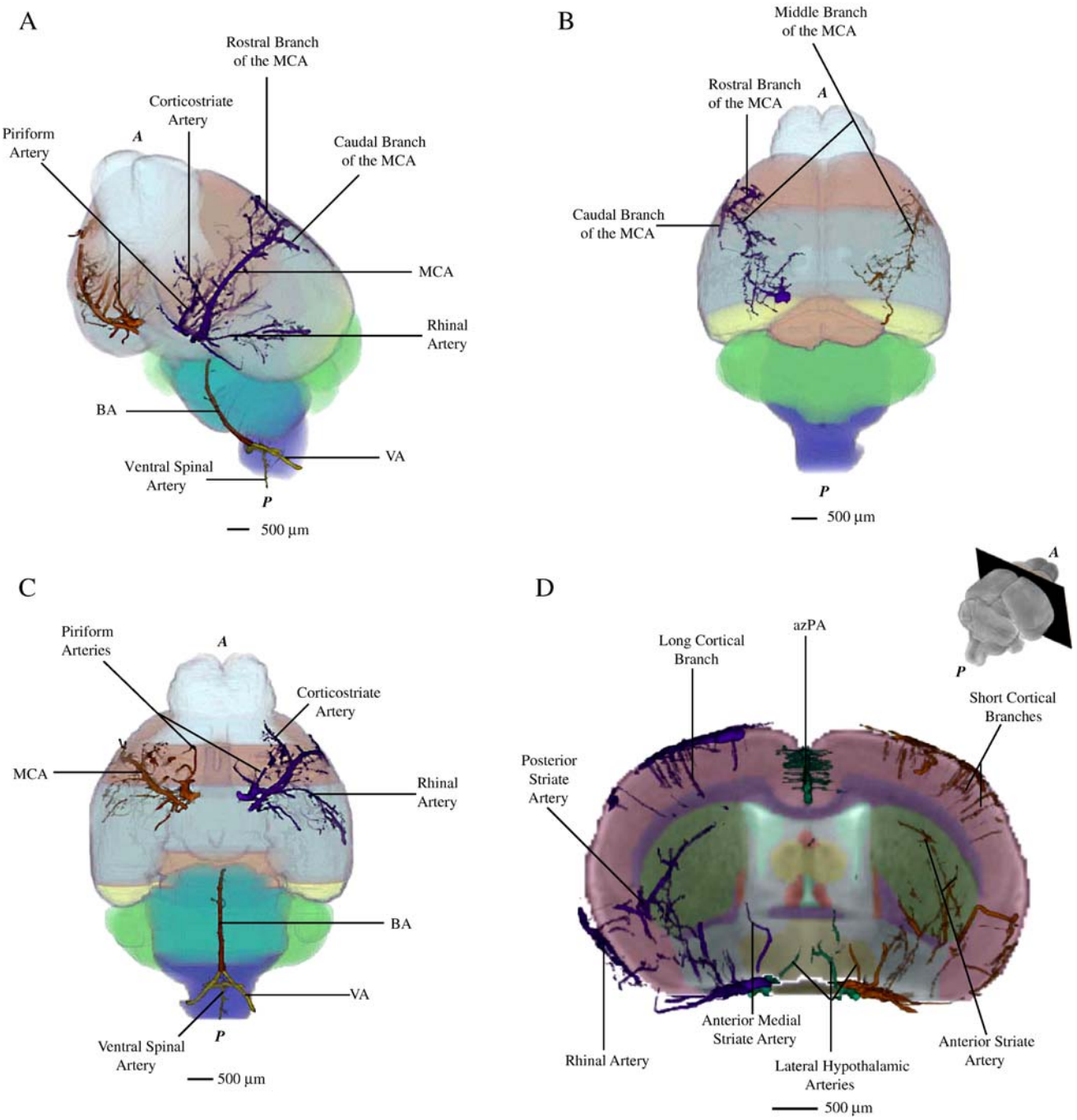

Fig. 5. MCA, with VA and BA, on brain surface with major lobar regions depicted, and MCA on coronal slice plane. (A) Brain surface showing the inferior, frontal, and lateral aspects of the MCA. BA and VA are also visible. (B) MCA on brain surface, superior view. (C) MCA, VA and BA on brain surface, inferior view. (D) Coronal slice plane showing the MCA, at or near the MCA anatomical location, posterior view, insert represents the level at which the slice was taken.

colliculi anterior to the sigmoid sinus. The lateral collicular vein is joined by the **longitudinal hippocampal vein** (Fig. 7C), which drains the hippocampus parallel to the longitudinal hippocampal artery. Located superior to the longitudinal hippocampal veins is the **great cerebral vein of Galen** (Fig. 7C) which runs posteriorly along the interior–midline of the cerebrum, in between the posterior hippocampi and below the posterior corpus callosum. This vein joins the aggregation of sinuses where the superior sagittal sinus, the transverse sinus, and the longitudinal hippocampal arteries join. The **thalamostriate vein** (Fig. 7C) joins the great cerebral vein of Galen anteriorly. They drain the thalamus and striatum from the dorsal aspect, just inferior to the hippocampus.

Discussion

We present here the detailed cerebral vasculature anatomy of the mouse using a combination of high-resolution MRI and microCT which is an efficient alternative to in vitro stereological approaches. We believe all of the major named vessels were

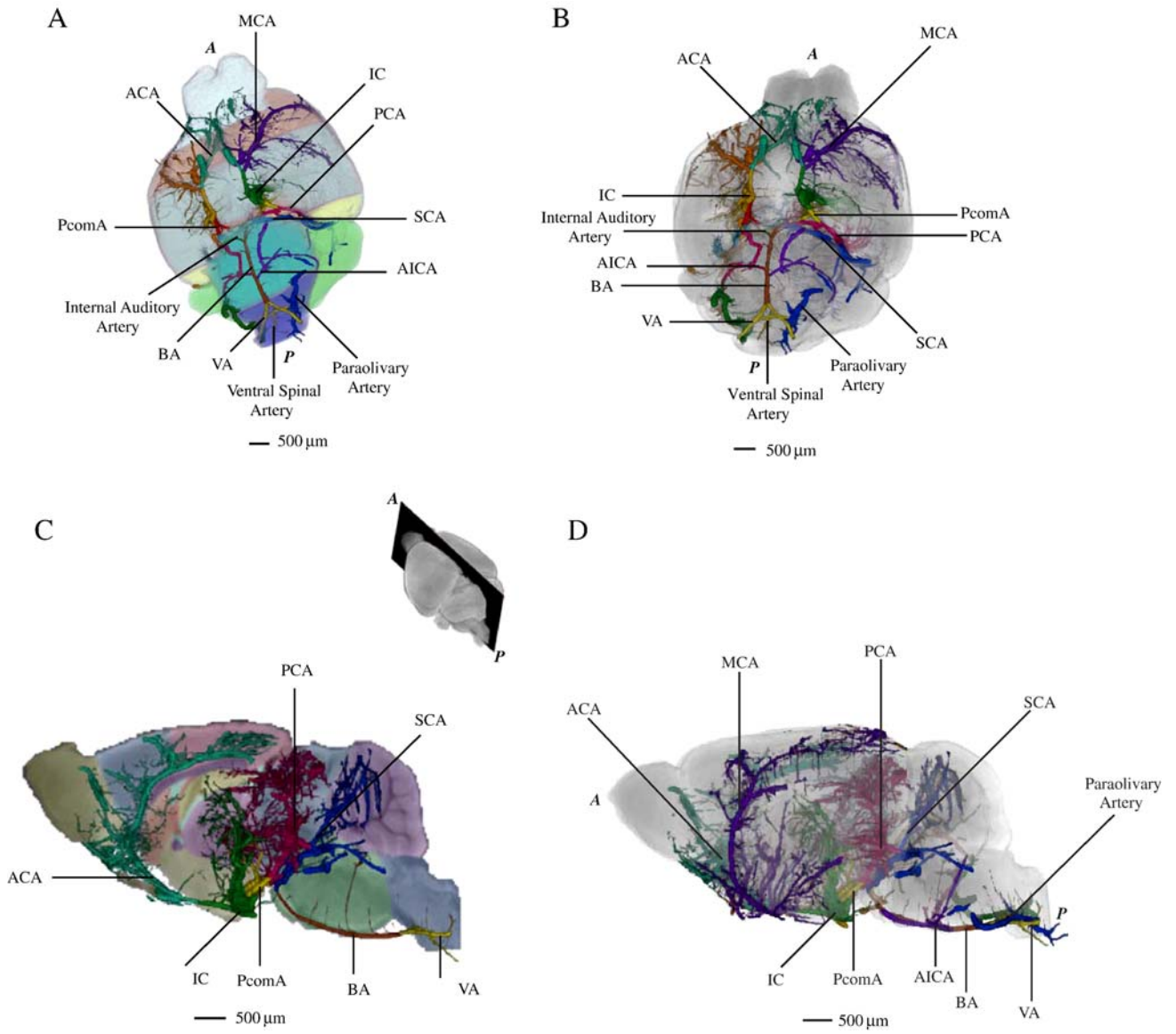

Fig. 6. Circle of Willis on mouse brain surface, and all arteries on brain surface and a slice plane. (A) Circle of Willis on mouse brain surface with lobar regions depicted. The brain is shown from the inferior view at a small angle, enabling the best view possible of all arteries involved in the Circle of Willis. (B) Circle of Willis on semi-transparent mouse surface, also viewed inferiorly from an angle. (C) Arteries superimposed on a sagittal slice, midline. Insert represents the level at which the slice was taken. The MCA is excluded to allow better viewing of the internal arteries. (D) All major cerebral arteries with a semi-transparent mouse brain surface, left view.

present and perfused with contrast agent for the specimen used to create the atlas. We make this inference based on the absence of obvious imaging artifacts, the consistency of the vessel anatomy between the different specimens, and the manner in which the vessel network fills the entire volume of the brain. There may however be some inaccuracy in the diameter of vessels. This is because the perfused contrast agent hardens in vessels at a uniform pressure whereas in the in vivo system pressure drops between the arterial and venous ends of the circulation potentially causing arterial and venous diameters in the fixed specimen to be under- and overestimated, respectively.

With respect to inter-specimen variability all four mice from this study showed all of the vessels described in the manuscript with the exception of a few of the superficial veins which were accidentally torn during the removal of the skull. While this study did not examine strain differences, the presented atlas is likely to apply with little modification to other mouse strains. Of note is that differences in the posterior communicating artery have been reported between strains (Barone et al., 1993). In addition, this artery in the C57BL/6 strain has been reported to be absent or poorly formed in some specimens.

While vascular atlases of other rodents related to mouse, such as rat and guinea pigs exist, we found a number of specific vascular differences between mice and these two rodents, rabbits (which share subclass with mice) and humans. These differences are briefly discussed below.

Mouse is most closely related to rats and as such, the CBA mouse vasculature was found to be very similar in pattern to that

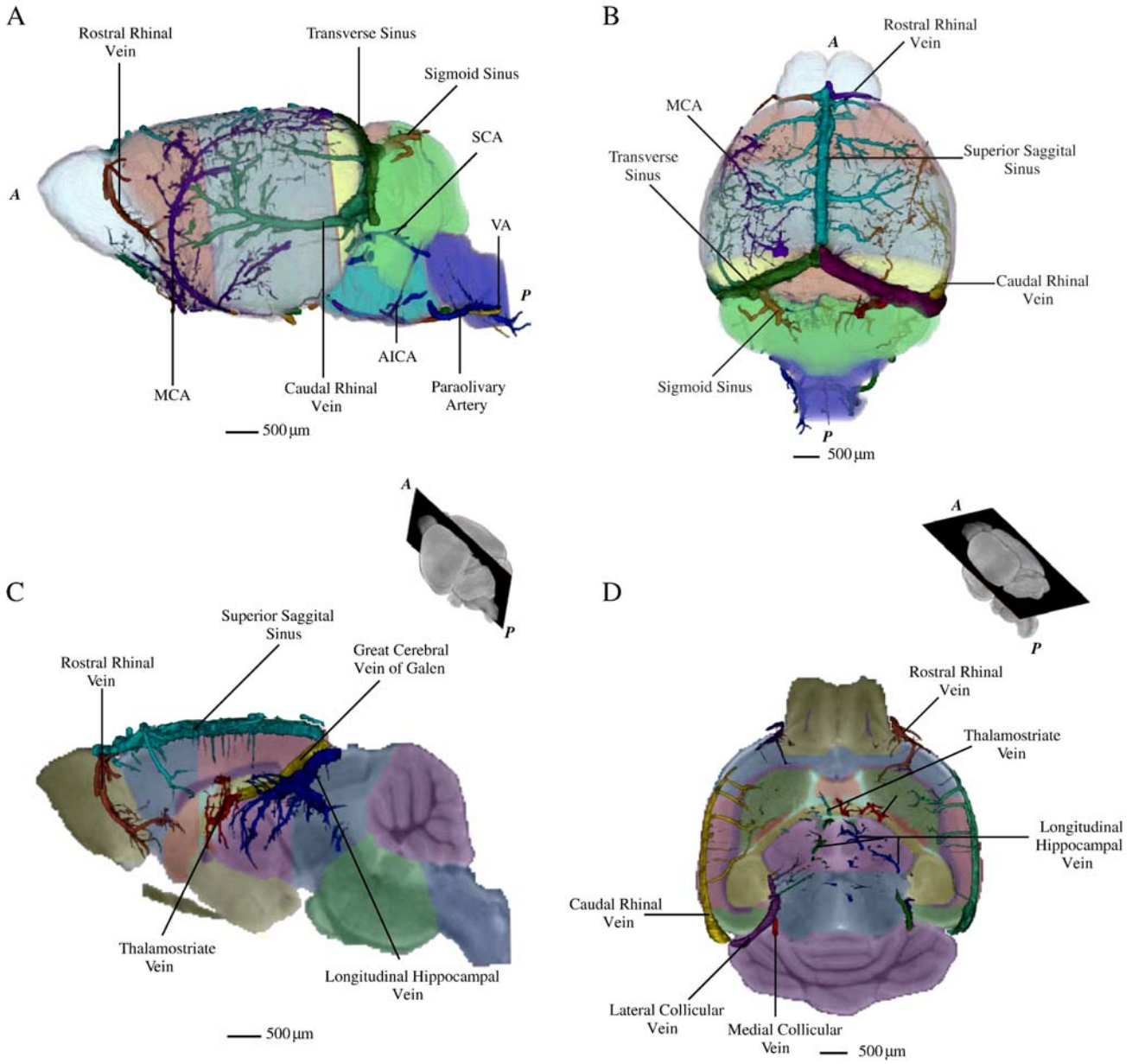

Fig. 7. Veins on mouse brain surface and slice planes. Inserts represent the level at which the slice of interest was taken. (A) Veins superimposed on mouse brain surface with lobar regions depicted, left view. Surface arteries, such as the MCA, VA, AICA, and paraolivary artery, are also visible. (B) Veins superimposed on mouse brain surface with lobar regions depicted, superior view. The MCA is also visible. (C) Sagittal slice plane, midline, showing the internal veins, as seen from the left view. (D) Horizontal slice plane showing major veins, inferior view.

described by Scremin (1995) with one exception. The termination point of the posterior communicating artery in mice is located shortly after the posterior cerebral artery emerges from the superior cerebellar artery (SCA). In comparison, the rat PcomA tends to join the PCA at a point which is located more distal (Brown, 1966) and is longer in rats than mouse.

The mouse vasculature differs more from the guinea pig than the rat. Unlike mice, guinea pigs have two posterior cerebral arteries on each side, namely, the rostral and caudal PCA (Librizzi et al., 1999; Nilges, 1944). Second, the internal carotid in the guinea pig joins the circle of Willis close to the middle cerebral artery (Librizzi et al., 1999; Nilges, 1944; Majewska-Michalska, 1994), similar to human brain vasculature (Nolte, 1998). In addition, the nomenclature differs slightly such that the 'ventral' spinal artery, which comes off the vertebral in mouse and rat, is called the 'anterior' spinal artery in guinea pigs (Majewska-Michalska, 1994). In terms of blood supply to brain structures, while mouse, rat and guinea pigs are similar, one striking difference is that in guinea pigs, the choroid artery of the IC supplies a wider ranges of structures including the putamen, caudate nucleus, and globus pallidus (Majewska-Michalska, 1994), while the mouse shows only sparse anterior choroid vasculature around the left globus pallidus, with the MCA being the major blood supply to there areas. The MCA supplies some of the thalamus in guinea pigs (Majewska-Michalska, 1994) while in mice the thalamus is supplied predominately by the anterior choroid artery and the PCA.

Although the rabbit belongs to the same subclass, Eutheria, it is of a different phylogenic order (lagomorpha) (Wilson and Reeder, 2006) and differs from the rodent vasculature. The IC joins the circle of Willis behind the MCA, further posterior than the point where the mouse IC joins the circle (Prolo and Stilwell, 1962). The IC gives off inferior hypophysial arteries medially, as well as ophthalmic arteries directed anteriorly, which are not visible in the mouse. The lateral and medial striate arteries in rabbit arise both from the IC and from the MCA, instead of solely from the MCA which is the case in mouse. Moreover, the anterior choroid artery of the IC not only supplies the thalamus and the choroid plexus, as in the mouse, but portions of the hippocampus as well (Prolo and Stilwell, 1962). An artery is given off the ACA just anterior to the MCA on the circle of Willis which is not present in rodents, called the recurrent branch of Heubner. This artery parallels the course of the MCA over the convexity of the rabbit brain and is considered an accessory of the MCA (Prolo and Stilwell, 1962). Rabbits are, however, similar to rodents in that the ACAs fuse to form a single azACA. Occasionally an anterior communicating artery is noticed before the ACA fusion (Prolo and Stilwell, 1962). The rabbit PcomA is very long in comparison to the mouse and rat. Posteromedial and posterolateral perforating vessels branch off the PcomA to supply mostly the hypothalamus and ventral thalamus, respectively (Prolo and Stilwell, 1962). They appear to be similar to the lateral hypothalamic arteries and ventral thalamic arteries seen branching off of the PcomA in the mouse. A large branch of the PCA, termed the periventricular ramus, is seen in rabbit near the posterolateral vessels that is not seen in the mouse (Prolo and Stilwell, 1962). The PCA gives off perforating posteromedial vessels supplying the posterior hypothalamus, and perforating posterolateral vessels supplying the substantia nigra and subthalamus (Prolo and Stilwell, 1962). Shortly after the PCA meets the PcomA, it gives off the mesencephalic and thalamogeniculate arteries. The mesencephalic artery supplies the anterior midbrain (mostly the superior cerebellar peduncle and colliculi). The thalamogeniculate artery gives lateral branches to the hippocampus, similar to the longitudinal hippocampal artery in mice, and finally branches into the geniculate and thalamic arteries. The geniculate artery supplies the more posterior aspect of the thalamus, along with cortical branches to the surrounding occipital and parietal lobes. The thalamic artery penetrates the thalamus superiorly, feeding the top portion of the thalamus (Prolo and Stilwell, 1962). At the BA bifurcation, posteromedial vessels supply the anterior midbrain, the posterior ventral thalamus, and the posterior dorsal hypothalamus (Prolo and Stilwell, 1962).

The human cerebral arterial network differs in a number of respects from the mouse. The same major arteries are involved in the circle of Willis; however, the complexity of the human brain versus the mouse brain leads to a different arterial pattern. The IC, the major blood provider to the cerebrum, branches off into the ACA medially and the MCA laterally as soon as it joins the cerebrum. In addition, the IC gives off a thin AchA, which supplies not only the choroid plexus and thalamus as in mice, but also the hippocampus (Montemurro and Bruni, 1988). Two ACAs head anteriorly from either IC, connected by an anterior communicating artery, but otherwise remain separate throughout their extent in the cerebrum. The ACA gives off a number of perforating arteries (also called ganglionic arteries) that penetrate the brain through the anterior perforating substance on the base of the brain near the optic chiasm. These arteries supply the hypothalamus, putamen, and caudate nucleus (Montemurro and Bruni, 1988). The ACA gives off the recurrent artery of Heubner laterally, near the region of the anterior communicating artery, which feeds the basal ganglia and anterior portions of the internal capsule (Heimer, 1995). The ACAs enter the longitudinal fissure to travel in front and on top of the corpus callosum. At the ventral base of the corpus callosum, the ACA gives off the frontopolar branch directed medial and anteriorly (Montemurro and Bruni, 1988), similar to the medial orbitofrontal artery in mice. Each ACA split at the superior anterior limit of the corpus callosum into the pericallosal artery and the callosomarginal artery (Nolte, 1998). The pericallosal arteries follow the superior aspect of the corpus callosum, much like the azPA in the mouse. The callosomarginal artery travels along the human cingulate sulcus; an equivalent of this artery is not seen in mice. The MCA gives off many perforating, or striate, arteries that perforate the brain in the anterior perforating substance to supply the striatum, portions of the globus pallidus, hypothalamus, and parts of the internal capsule (Montemurro and Bruni, 1988; Nolte, 1998). The main trunk of the MCA travels laterally around the brain in the lateral fissure, where it gives off numerous branches to feed the lateral aspects of the frontal, parietal, occipital, and temporal lobes, as well as the temporal pole (Montemurro and Bruni, 1988; Nolte, 1998). Behind the MCA, the IC gives off the PcomA, which is a very thin artery in the human. It connects posteriorly with the PCA, the terminal branch of the BA, near the origin of the PCA from the BA (Montemurro and Bruni, 1988; Nolte, 1998). The PCA supplies the cortex of the majority of the occipital lobe, and the inferior and medial aspect of the temporal lobe. The PCA gives off perforating arteries near its origin from the BA that penetrate the posterior perforating substance near the mammillary bodies to supply the hypothalamus, thalamus, and midbrain (Montemurro and Bruni, 1988; Nolte, 1998). The PCA also supplies the hippocampus as well as the choroid plexus (Heimer, 1995; Nolte, 1998). The SCA branches off the BA just behind the PCA. It feeds the midbrain, superior cerebellum and portions of the pons (Montemurro and Bruni, 1988; Nolte, 1998). The BA gives off internal auditory arteries as well as the anterior inferior cerebellar artery, while the vertebral arteries give off the posterior inferior cerebellar arteries laterally, and the anterior spinal artery (Heimer, 1995; Nolte, 1998), the latter being equivalent to the ventral spinal artery in mice.

In conclusion, this article provides a standard basic mouse cerebral vascular anatomy for major arteries and branches that can be visualized with the resolution available from microCT. There are a number of mammals where vasculature anatomy has been extensively studied, and while the rat proved to be very close anatomically to the mouse, there are some differences. In the course of this project, the main arteries and many of the major branches were delineated and correctly identified with knowledge of the brain structures these arteries supply which will prove useful for future studies involving mouse cerebral vasculature. The atlas created here will be made freely available to other researchers upon request.

Acknowledgments

This research was funded by Sunnybrook Research Institute Start up Funds, Ontario Research and Development Challenge Fund and the Canada Foundation for Innovation. We would like to acknowledge the efforts of Shoshana Spring and Lisa Yu in preparing and imaging the specimens.

References

Barone, F.C., Knudsen, D.J., Nelson, A.H., Feuerstein, G.Z., Willette, R.N., 1993. Mouse strain differences in susceptibility to cerebral ischemia are related to cerebral vascular anatomy. J. Cereb. Blood Flow Metab. 13, 683–692.

Beckmann, N., 2000. High resolution magnetic resonance angiography non-invasively reveals mouse strain differences in the cerebrovascular anatomy in vivo. Magn. Reson. Med. 44, 252–258.

Beckmann, N., Stirnimann, R., Bochelen, D., 1999. High-resolution magnetic resonance angiography of the mouse brain: application to murine focal cerebral ischemia models. J. Magn. Reson. 140, 442–450.

Beckmann, N., Schuler, A., Mueggler, T., Meyer, E.P., Wiederhold, K.H., Staufenbiel, M., Krucker, T., 2003. Age-dependent cerebrovascular abnormalities and blood flow disturbances in APP23 mice modeling Alzheimer's disease. J. Neurosci. 23, 8453–8459.

Brown, J.O., 1966. The morphology of circulus arteriosus cerebri in rats. Anat. Rec. 156, 99–106.

Cook, M.J., 1965. The Anatomy of the Laboratory Mouse. Acedemic Press, New York.

Franklin, K.B.J., Paxinos, G., 2001. The Mouse Brain in Stereotaxic Coordinates, 2nd ed. Academic Press, San Diego.

Greene, E., 1955. Anatomy of the Rat. Hafner Pub. Co., New York.

Heimer, L., 1995. The Human Brain and Spinal Cord: Functional Neuroanatomy and Dissection Guide, 2nd ed. Springer-Verlag, New York.

Henkelman, R.M., Dazai, J., Lifshitz, N., Nieman, B.J., Tsatskis, S., Lerch, J., Bishop, J., Kale, S., Sled, J.G., Chen, X.J., 2006. High throughput microimaging of the mouse brain. International Society of Magnetic Resonance in Medicine, 14th Scientific Meeting.

Jorgensen, S.M., Demirkaya, O., Ritman, E.L., 1998. Three-dimensional imaging of vasculature and parenchyma in intact rodent organs with X-ray micro-CT. Am. J. Physiol. 275, H1103–H1114.

Kitagawa, K., Matsumoto, M., Yang, G., Mabuchi, T., Yagita, Y., Hori, M., Yanagihara, T., 1998. Cerebral ischemia after bilateral carotid artery occlusion and intraluminal suture occlusion in mice: evaluation of the patency of the posterior communicating artery. J. Cereb. Blood Flow Metab. 18, 570–579.

Kovacevic, N., Henderson, J.T., Chan, E., Lifshitz, N., Bishop, J., Evans, A.C., Henkelman, R.M., Chen, X.J., 2005. A three-dimensional MRI atlas of the mouse brain with estimates of the average and variability. Cereb. Cortex 15, 639–645.

Krucker, T., Schuler, A., Meyer, E.P., Staufenbiel, M., Beckmann, N., 2004. Magnetic resonance angiography and vascular corrosion casting as tools in biomedical research: application to transgenic mice modeling Alzheimer's disease. Neurol. Res. 26, 507–516.

Librizzi, L., Biella, G., Cimino, C., De, C.M., 1999. Arterial supply of limbic structures in the guinea pig. J. Comp. Neurol. 411, 674–682.

Lin, W., Abendschein, D.R., Celik, A., Dolan, R.P., Lauffer, R.B., Walovitch, R.C., Haacke, E.M., 1997. Intravascular contrast agent improves magnetic resonance angiography of carotid arteries in minipigs. J. Magn. Reson. Imaging 7, 963–971.

Ma, Y., Hof, P.R., Grant, S.C., Blackband, S.J., Bennett, R., Slatest, L., McGuigan, M.D., Benveniste, H., 2005. A three-dimensional digital atlas database of the adult C57BL/6J mouse brain by magnetic resonance microscopy. Neuroscience 135, 1203–1215.

Maeda, K., Hata, R., Hossmann, K.A., 1998. Differences in the cerebrovascular anatomy of C57black/6 and SV129 mice. Neuroreport 9, 1317–1319.

Majewska-Michalska, E., 1994. Vascularization of the brain in guinea pig: I. Gross anatomy of the arteries and veins. Folia Morphol. (Warsz.) 53, 249–268.

Majewska-Michalska, E., 1995. Vascularization of the brain in guinea pig: II. Regions of vascular supply and spatial topography of the arteries in particular parts of the brain. Folia Morphol. (Warsz.) 54, 33–40.

Majewska-Michalska, E., 1997a. Vascularization of the brain in guinea pig: III. Vascular architecture of the medulla oblongata, pons, and cerebellum. Folia Morphol. (Warsz.) 56, 41–46.

Majewska-Michalska, E., 1997b. Vascularization of the brain in guinea pig: IV. Angioarchitectonics of the tectum, tegmentum, and crura mescencephali. Folia Morphol. (Warsz.) 56, 47–53.

Majewska-Michalska, E., 1997c. Vascularization of the brain in guinea pig: V. Angioarchitectonics of the thalamus, telencephalon and internal capsule. Folia Morphol. (Warsz.) 56, 55–62.

Majewska-Michalska, E., 1998. The vertebrobasilar arterial system in guinea pig as compared with dog and human. Folia Morphol. (Warsz.) 57, 121–131.

Marxen, M., Thornton, M.M., Chiarot, C.B., Klement, G., Koprivnikar, J., Sled, J.G., Henkelman, R.M., 2004. MicroCT scanner performance and considerations for vascular specimen imaging. Med. Phys. 31, 305–313.

Miraux, S., Serres, S., Thiaudiere, E., Canioni, P., Merle, M., Franconi, J.M., 2004. Gadolinium-enhanced small-animal TOF magnetic resonance angiography. MAGMA 17, 348–352.

Montemurro, D.G., Bruni, J.E., 1988. Blood supply of the brain. In: Montemurro, D.G. (Ed.), The Human Brain in Dissection. Oxford University Press, New York, pp. 26–31.

Nieman, B.J., Bock, N.A., Bishop, J., Sled, J.G., Chen, X.J., Henkelman, R.M., 2005. Fast spin-echo for multiple mouse magnetic resonance phenotyping. Magn. Reson. Med. 54, 532–537.

Nilges, R., 1944. The arteries of the mammalian *Cornu ammonis*. J. Comp. Neurol. 80, 177–190.

Nolte, J., 1998. Blood supply of the brain. In: Nolte, J. (Ed.), The Human Brain: An Introduction to its Functional Anatomy. Mosby, St. Louis, pp. 117–143.

Ohtake, M., Morino, S., Kaidoh, T., Inoue, T., 2004. Three-dimensional structural changes in cerebral microvessels after transient focal cerebral ischemia in rats: scanning electron microscopic study of corrosion casts. Neuropathology 24, 219–227.

Okuyama, S., Okuyama, J., Okuyama, J., Tamatsu, Y., Shimada, K., Hoshi, H., Iwai, J., 2004. The arterial circle of Willis of the mouse helps to decipher secrets of cerebral vascular accidents in the human. Med. Hypotheses 63, 997–1009.

Prolo, D., Stilwell, D., 1962. Arterial supply of the diencephalon and some associated areas of the rabbit brain. J. Comp. Neurol. 119, 229–254.

Reese, T., Bochelen, D., Sauter, A., Beckmann, N., Rudin, M., 1999. Magnetic resonance angiography of the rat cerebrovascular system without the use of contrast agents. NMR Biomed. 12, 189–196.

Scremin, O.U., 1995. Cerebral vascular system. In: Paxinos, G. (Ed.), The Rat Nervous System. Academic Press, San Diego, pp. 3–35.

Ward, R., Collins, R.L., Tanguay, G., Miceli, D., 1990. A quantitative study of cerebrovascular variation in inbred mice. J. Anat. 173, 87–95.

Wilson, D.E., Reeder, D.A., 2006. Mammal Species of the World: A Taxonomic and Geographic Reference, 3rd ed. Johns Hopkins University Press, Baltimore.